CHINESE OPTICS LETTERS

Vol. 20, No. 11 | November 2022

Second-order cumulants ghost imaging

Huan Zhao (赵 环)[1], Xiaoqian Wang (王晓茜)[1**], Chao Gao (高 超)[1], Zhuo Yu (于 卓)[1,2], Shuang Wang (王 爽)[1], Lidan Gou (苟立丹)[1], and Zhihai Yao (姚治海)[1*]

[1] Department of Physics, Changchun University of Science and Technology, Changchun 130022, China

[2] School of Physics and Electronics, Baicheng Normal University, Baicheng 137000, China

*Corresponding author: yaozh@cust.edu.cn

**Corresponding author: xqwang21@163.com

Received April 21, 2022 | Accepted June 15, 2022 | Posted Online July 21, 2022

Ghost imaging (GI) is a technique to retrieve images by correlating intensity fluctuations. In this Letter, we present a novel scheme for GI referred to as second-order cumulants GI (SCGI). The image is retrieved from fluctuation information, and resolution may be enhanced compared to traditional GI. We experimentally performed SCGI image reconstruction, and the results are in agreement with theoretical predictions.

Keywords: ghost imaging; cumulants; resolution.

DOI: 10.3788/COL202220.112602

1. Introduction

Ghost imaging (GI) is an imaging technique based on second-order intensity correlation[1–10]. GI has many advantages compared to traditional imaging techniques. For example, thermal lens-less GI may be performed[11] even in the presence of atmospheric and instrumental fluctuations[12–16]. The resolution is an important factor in evaluating image quality[17,18], and how to improve the resolution of GI is a key factor in the development of GI[17–20].

The spatial resolution of a GI system is limited by the point spread function (PSF) of the system, just as in traditional imaging[18]. In general, the resolution of GI is taken to be the full width at half-maximum (FWHM) of the PSF, which itself is approximately equal to the average size of the speckles[18]. In traditional imaging systems, many schemes have been proposed to improve resolution via reducing the impact of PSF[21,22]. Some schemes to improve the resolution of GI have also been proposed. Compressed sensing GI (CSGI) reduces the effect of PSF on the imaging quality using sparsity constraints to improve resolution[23–28]. Han's group reported a proof-of-principle experiment, where the resolution of a thermal light two-arm microscope scheme is improved by employing second-order intensity correlation imaging to narrow PSF[29]. The scheme has been implemented based on high-pass spatial-frequency filtering of the correlated intensity fluctuations[30]. The narrowing of PSF by higher-order correlation of non-Rayleigh speckle fields has been reported[31]. Other schemes to enhance the resolution of GI have also been suggested, such as spatial low-pass filtering[18,20], localizing and thresholding[32], preconditioned deconvolution methods[33], optical random speckle encoding based on hybrid wavelength and phase modulation scheme[34], deep neural network constraints[35], and speeded up robust features new sum of modified Laplacian (SURF-NSML)[36].

In this Letter, we put forward a novel scheme to enhance the resolution of GI by narrowing the PSF, referred to as second-order cumulants GI (SCGI). In our scheme, the fluctuation information of GI is exploited, which contains more information than traditional GI data and allows one to improve the resolution. We theoretically analyze the feasibility of the scheme and its performance in improving the resolution by second-order cumulants and experimentally verify results using a double-slit object. We also show that second-order cumulants can be used together with other modified GI schemes, such as CSGI, to obtain images with higher resolution.

2. Methods

A typical GI experimental setup is shown in Fig. 1, where a double-slit object is employed to assess the resolution[29,37,38]. In this system, there is a monochromatic source of light at wavelength λ. A light beam from the source propagates to the object through an optical system with a PSF:

$$h(x,\alpha) = \frac{e^{-ikz}}{i\lambda z}\exp\left[\frac{-i\pi}{\lambda z}(x-\alpha)^2\right], \tag{1}$$

where $k = \frac{2\pi}{\lambda}$, and z is the distance between the source and the object. x and α are the transverse coordinates on the source and the object plane, respectively. The light field at the object plane is

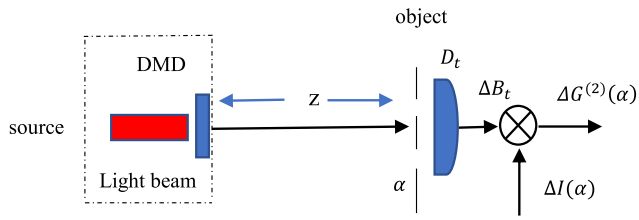

Fig. 1. Experimental setup to assess the resolution of GI. There is a digital micro-mirror device (DMD) in the source. The light illuminates the object and then is collected by a bucket detector (D_t) with no spatial resolution.

$$E(\alpha) = \int E(x)h(x,\alpha)\mathrm{d}x, \tag{2}$$

where $E(x)$ denotes the light field of source plane at x. The light intensity at the object plane is

$$I(\alpha) = E^*(\alpha)E(\alpha). \tag{3}$$

If $T(\alpha)$ represents the light field transmission function of the object, the light intensity at the bucket detector is given by

$$B_t = \int I(\alpha)|T(\alpha)|^2\mathrm{d}\alpha. \tag{4}$$

The intensity fluctuations correlation between $I(\alpha)$ and B_t is

$$\begin{aligned}\Delta G^{(2)}(\alpha) &= \langle \Delta I(\alpha)\Delta B_t\rangle = \langle [I(\alpha) - \langle I(\alpha)\rangle][B_t - \langle B_t\rangle]\rangle \\ &= \left\langle [I(\alpha) - \langle I(\alpha)\rangle]\left[\int I(\alpha')|T(\alpha')|^2\mathrm{d}\alpha' \right.\right. \\ &\quad \left.\left. - \left\langle \int I(\alpha')|T(\alpha')|^2\mathrm{d}\alpha'\right\rangle\right]\right\rangle \\ &= \int \left|\int G^{(1)}(x,x')T(\alpha')h^*(x,\alpha)h(x',\alpha')\mathrm{d}x\mathrm{d}x'\right|^2 \mathrm{d}\alpha',\end{aligned} \tag{5}$$

where $\langle\cdots\rangle$ represents the ensemble average, and $G^{(1)}(x,x') = \langle E^*(x)E(x')\rangle$ is the first-order correlation function at the source. We consider a situation where light comes as a point-like source and is randomly and uniformly distributed on the source plane. If the light spot is located at x_0, we have $G^{(1)}(x,x_0) = I_0\delta(x - x_0)$, where I_0 is the intensity of the source. Substituting $G^{(1)}(x,x')$ and Eq. (1) into Eq. (5), after some calculations, we arrive at

$$\Delta G^{(2)}(\alpha) = I_0^2 \int |T(\alpha')|^2 \operatorname{sinc}^2\left[\frac{2\pi R}{\lambda z}(\alpha - \alpha')\right]\mathrm{d}\alpha', \tag{6}$$

where R is the radius of the light source. Obviously, the image resolution is constrained by this PSF, and the resolution is determined by the first zero of the sinc^2 function in Eq. (6).

I_0 is usually assumed constant in traditional GI, i.e., one assumes that the emitting power of the light source is perfectly stable. In fact, the emitting power of the light source cannot be kept stable. Thus, $\Delta G^{(2)}(\alpha)$ in Eq. (6) should be substituted with $\Delta G^{(2)}(I_0,\alpha)$. Fluctuations of I_0 lead to fluctuations of $\Delta G^{(2)}(I_0,\alpha)$. We use the concept of cumulants to describe the fluctuations of $\Delta G^{(2)}(I_0,\alpha)$ since they contain more information than $\Delta G^{(2)}(I_0,\alpha)$ itself. The cumulant-generating function $K(s,\alpha)$ is defined as

$$\begin{aligned}K(s,\alpha) &= \ln\{\langle \exp[s\Delta G^{(2)}(I_0,\alpha)]\rangle\} = \sum_{n=1}^{\infty}\kappa_n(\alpha)\frac{s^n}{n!} \\ &= \mu(\alpha)\times s + \sigma^2(\alpha)\times\frac{s^2}{2} + \cdots,\end{aligned} \tag{7}$$

where $\kappa_n(\alpha)$ is the nth-order cumulants, $\mu(\alpha) = \langle \Delta G^{(2)}(I_0,\alpha)\rangle$, and $\sigma(\beta) = \langle \Delta G^{(2)}(I_0,\alpha) - \langle \Delta G^{(2)}(I_0,\alpha)\rangle\rangle$. The nth-order cumulant is given by

$$\kappa_n(\alpha) = \left.\frac{\mathrm{d}^{(n)}K(s,\alpha)}{\mathrm{d}s^{(n)}}\right|_{s=0}. \tag{8}$$

In order to minimize the imaging time, we consider the second-order cumulants, which can be written as

$$\begin{aligned}\kappa_2(\alpha) &= \langle [\Delta G^{(2)}(I_0,\alpha) - \langle \Delta G^{(2)}(I_0,\alpha)\rangle]^2\rangle \\ &= \int \kappa_2(\alpha,\alpha')\mathrm{d}\alpha' + L(\alpha),\end{aligned} \tag{9}$$

where

$$\begin{aligned}\kappa_2(\alpha,\alpha') &= \langle [\Delta G^{(2)}(I_0,\alpha,\alpha') - \langle \Delta G^{(2)}(I_0,\alpha,\alpha')\rangle]^2\rangle \\ &= \langle (I_0^2 - \langle I_0^2\rangle)^2\rangle \times |T(\alpha')|^4 \times \operatorname{sinc}^4\left[\frac{2\pi R}{\lambda z}(\alpha - \alpha')\right],\end{aligned} \tag{10}$$

and

$$\begin{aligned}L(\alpha) &= \int_{\alpha'}\int_{\alpha''\neq\alpha'} \langle [\Delta G^{(2)}(I_0,\alpha,\alpha') \\ &\quad - \langle \Delta G^{(2)}(I_0,\alpha,\alpha')\rangle][\Delta G^{(2)}(I_0,\alpha,\alpha'') \\ &\quad - \langle \Delta G^{(2)}(I_0,\alpha,\alpha'')\rangle]\rangle \mathrm{d}\alpha'\mathrm{d}\alpha'' \\ &= \langle (I_0^2 - \langle I_0^2\rangle)^2\rangle \times \int_{\alpha'}\int_{\alpha''\neq\alpha'} |T(\alpha')|^2|T(\alpha'')|^2 \\ &\quad \times \operatorname{sinc}^2\left[\frac{2\pi R}{\lambda z}(\alpha - \alpha')\right]\operatorname{sinc}^2\left[\frac{2\pi R}{\lambda z}(\alpha - \alpha'')\right]\mathrm{d}\alpha'\mathrm{d}\alpha'',\end{aligned} \tag{11}$$

where $\Delta G^{(2)}(I_0,\alpha,\alpha') = I_0^2|T(\alpha')|^2 \operatorname{sinc}^2\left[\frac{2\pi R}{\lambda z}(\alpha - \alpha')\right]$ is the correlation between the intensity fluctuations at α and α'. As a matter of fact, $\kappa_2(\alpha)$ contains the information about fluctuations of $\Delta G^{(2)}(I_0,\alpha)$ and $\kappa_2(\alpha,\alpha')$ about those of $\Delta G^{(2)}(I_0,\alpha,\alpha')$. $L(\alpha)$ is the cross-information generated correlating $\Delta G^{(2)}(I_0,\alpha,\alpha') - \langle \Delta G^{(2)}(I_0,\alpha,\alpha')\rangle$ and $\Delta G^{(2)}(I_0,\alpha,\alpha'') - \langle \Delta G^{(2)}(I_0,\alpha,\alpha'')\rangle$ for all different α' and α'' ($\alpha' \neq \alpha''$). From Eq. (9), we see that $\kappa_2(\alpha)$ is written in terms of $\kappa_2(\alpha,\alpha')$ and $L(\alpha)$. According to Eqs. (10)

and (11), the FWHMs of $\kappa_2(\alpha,\alpha')$ and $L(\alpha)$ are influenced by z and λ. In particular, they increase with z or λ. One has $L(\alpha) = 0$ if there is no cross interference between any two points on the object plane. In the following, we make use of $\kappa_2(\alpha)$ instead of $\Delta G^{(2)}(I_0,\alpha)$ to reconstruct the image of the object, and, for this reason, we refer to our scheme as SCGI.

From Eqs. (9)–(11), we see that the intensity PSF of SCGI corresponds to a sinc^4 function, whereas in traditional GI the form of PSF scales as sinc^2. In turn, the FWHM of the PSF in Eq. (6) is larger than that in Eq. (9). In order to address a concrete example, we set $\lambda = 550$ nm, $z = 0.8$ m, and $R = 1$ mm. For a pinhole-like object at $\alpha' = 0$, the imaging results are shown in Fig. 2.

From Eq. (9), we see that $L(\alpha)$ affects the resolution of SCGI. In order to understand how, we consider a situation where the object is made of two pinholes placed at α' and $\alpha'' = -\alpha'$, respectively. The imaging results are shown in Fig. 3. Looking at Figs. 3(a) and 3(b), we see that the image of the object for $L(\alpha) = 0$ is clearer than for the case $L(\alpha) \neq 0$. This is because cross information, which cannot distinguish between $\kappa_2(\alpha,\alpha')$ and $\kappa_2(\alpha,\alpha'')$, is present when $L(\alpha) \neq 0$.

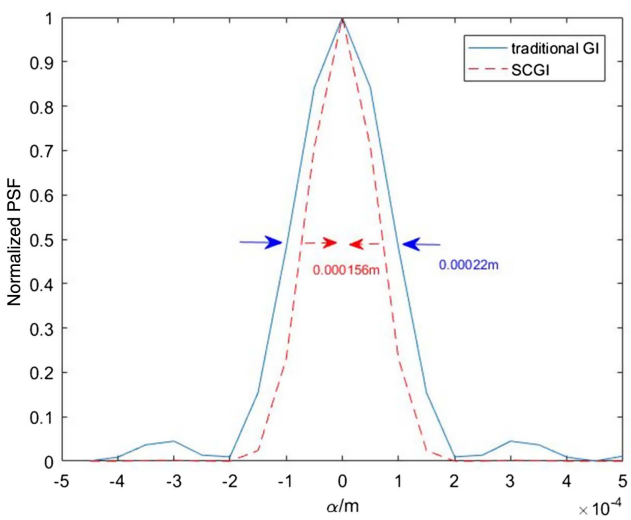

Fig. 2. PSF of a pinhole object at $\alpha' = 0$ for $\lambda = 550$ nm, $z = 0.8$ m, and $R = 0.001$ m by traditional GI (blue solid curve) and SCGI (red dash curve).

Compared to traditional GI, the resolution of SCGI improves even when $L(\alpha) \neq 0$. This may be seen as follows, using the Rayleigh criterion to assess the resolution of the GI[39], i.e., looking at the minimum separation between two incoherent point sources (α_0 and α_0', we set $\alpha_0 = -\alpha_0'$ for the sake of simplicity) that may be resolved into distinct objects[39]. For traditional GI, since the intensity PSF is a sinc^2 function, the Rayleigh distance is $d_1 = |\alpha_0 - \alpha_0'|$ when $\Delta G^{(2)}(I_0,0)/\Delta G^{(2)}(I_0,\alpha_0) \approx 0.81$ [we assume $|T(\alpha_0)|^2 = |T(-\alpha_0)|^2 = 1$]. On the other hand, from Eq. (9), we have that $\kappa_2(0)/\kappa_2(\alpha_0) = 0.6561 < 0.81$ for $d_1 = |\alpha_0 - \alpha_0'|$ by Eq. (9), i.e., SCGI shows enhanced resolution compared to traditional GI.

Second-order cumulants can also be used in other modified GI schemes, such as CSGI, which itself aims at improving the resolution of GI by reducing the effect of PSF on the information carried by $\Delta G^{(2)}(I_0,\alpha)$. $\kappa_2(\alpha)$ is the fluctuation information of $\Delta G^{(2)}(I_0,\alpha)$ and contains more information than $\Delta G^{(2)}(I_0,\alpha)$, such that it can be used in CSGI to further enhance the spatial resolution just as in traditional GI.

3. Results

We experimentally verify our theoretical predictions by using a computational GI setup. The light source is a projector (XE11F), and there is a digital mirror device (DMD) in the source. An optical spatial filter with a central wavelength of 550 nm is inserted in the light beam behind the projector. A bucket detector is composed of a lens and an optical detection circuit (LSSPD-2.5-3 P-08.26). The object is a double slit with width $a = 0.8$ mm, slits center distance $b = 1.2$ mm, and slit height

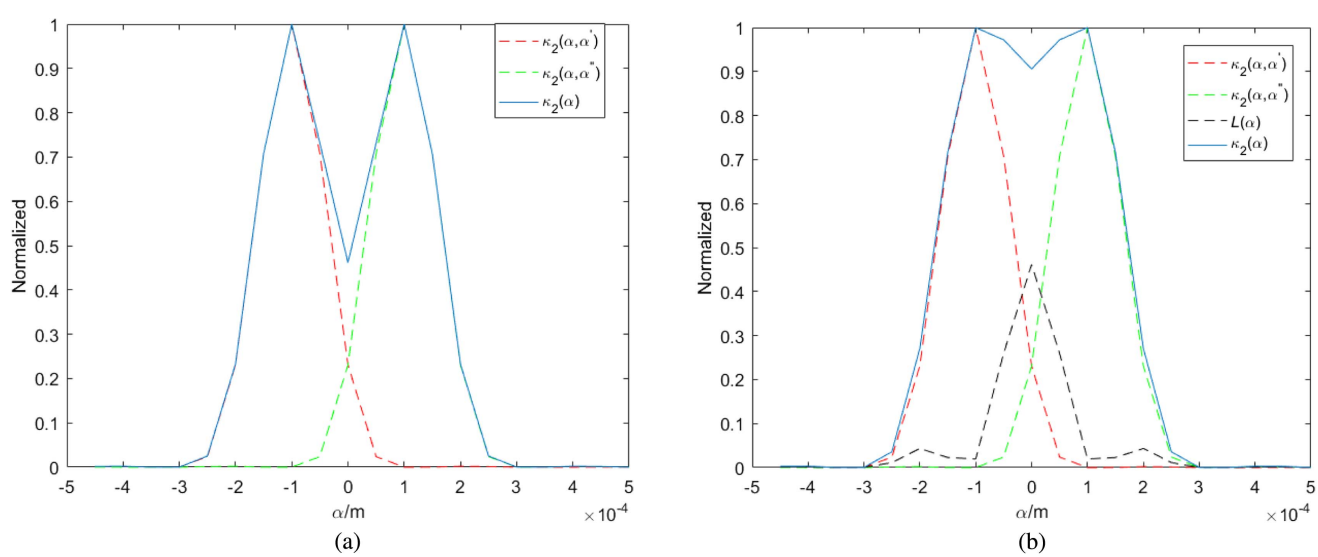

Fig. 3. Image of the two-pinhole object by SCGI when $\alpha' = -0.1$ mm, $\alpha'' = 0.1$ mm, $\lambda = 550$ nm, $R = 0.001$ m, and $z = 0.8$ m: (a) $L(\alpha) = 0$; (b) $L(\alpha) \neq 0$.

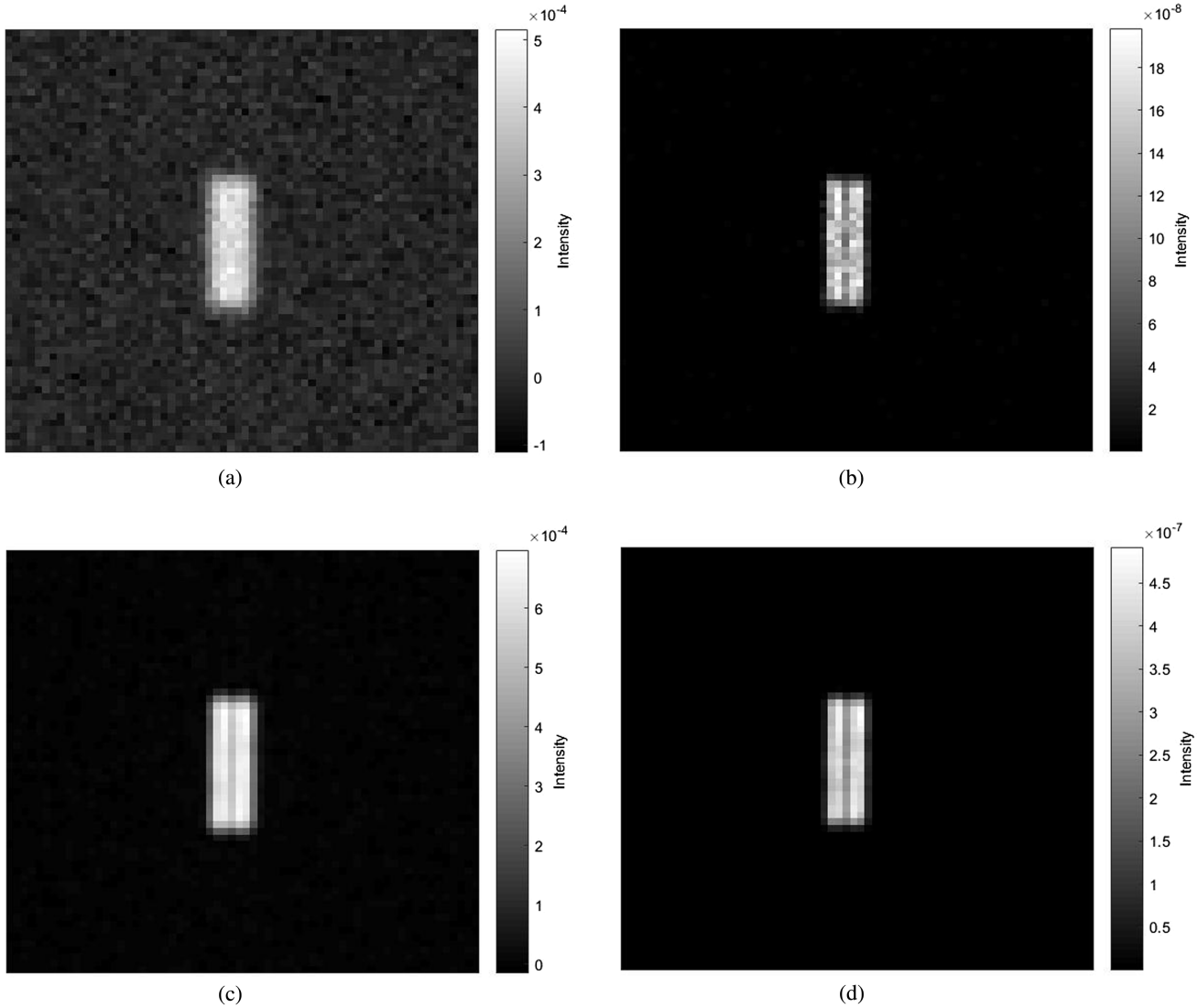

Fig. 4. Experimental results for a double slit: (a)–(d) show results by traditional GI, SCGI [$\kappa_2(\alpha)$ of traditional GI], CSGI, and SCGI [$\kappa_2(\alpha)$ of CSGI], respectively.

$g = 8$ mm. The distance between the source and the object is $z = 0.8$ m.

First, we demonstrate that second-order cumulants can be used in traditional GI to enhance the resolution. In particular, we measure the resolution of traditional GI and traditional GI with $\kappa_2(\alpha)$ in the same conditions. Results are obtained by averaging over 50,000 exposure frames. For $\kappa_2(\alpha)$, we get $\Delta G^{(2)}(I_0,\alpha)$ every 5000 steps. The experimental results are shown in Figs. 4(a) and 4(b). According to our theoretical analysis, the PSF of $\Delta G^{(2)}(I_0,\alpha)$ can be narrowed by $\kappa_2(\alpha)$. In Fig. 4(a), we find that the double slit cannot be distinguished. However, in Fig. 4(b), the double slit can be distinguished using $\kappa_2(\alpha)$. That means the PSF of $\Delta G^{(2)}(I_0,\alpha)$ is wider than the PSF of $\kappa_2(\alpha)$. The resolution obtained by $\kappa_2(\alpha)$ is improved compared to $\Delta G^{(2)}(I_0,\alpha)$. The experimental results are consistent with our theoretical analysis.

We then verify that second-order cumulants can also be used in other modified GI schemes. In particular, with the same setup, we prove experimentally that $\kappa_2(\alpha)$ can be used in the CSGI scheme. Here, for CSGI, we obtain $\Delta G^{(2)}(I_0,\alpha)$ with 3000 steps. Experimental results obtained by CSGI and CSGI with $\kappa_2(\alpha)$ are shown in Figs. 4(c) and 4(d), respectively. We see that the resolution obtained by CSGI with $\kappa_2(\alpha)$ is improved compared to CSGI.

4. Discussion

In conclusion, we have used $\kappa_2(\alpha)$ instead of $\Delta G^{(2)}(I_0,\alpha)$ to reconstruct the image of the object in the GI system. We have termed this protocol SCGI. Our theoretical analysis and experimental results show that the resolution of GI can be enhanced by SCGI without changing the experimental setup of GI. In order to verify the performance of the protocol, we applied $\kappa_2(\alpha)$ to the CSGI scheme and obtained images with higher resolution than those obtained by CSGI. Similarly, $\kappa_2(\alpha)$ can also be

used in other modified GI to enhance the resolution, such as spatial low-pass filter, localizing, and thresholding schemes. We will discuss them elsewhere.

Acknowledgement

This work was supported by the Science & Technology Development Project of Jilin Province (No. YDZJ202101ZYTS030).

References

1. T. B. Pittman, Y. H. Shih, D. V. Strekalov, and A. V. Sergienko, "Optical imaging by means of two-photon quantum entanglement," Phys. Rev. A **52**, R3429 (1995).
2. C. Gao, X.-Q. Wang, L.-D. Gou, Y.-L. Feng, H.-J. Cai, Z-F. Wang, and Z.-H. Yao, "Ghost imaging for an occluded object," Laser Phys. Lett. **16**, 065202 (2019).
3. C. Gao, X.-Q. Wang, Z.-F. Wang, Z. Li, G.-J. Du, F. Chang, and Z.-H. Yao, "Optimization of computational ghost imaging," Phys. Rev. A **96**, 023838 (2017).
4. A. Gatti, E. Brambilla, M. Bache, and L. A. Lugiato, "Ghost imaging with thermal light: comparing entanglement and classical correlation," Phys. Rev. Lett. **93**, 093602 (2004).
5. P. H. S. Ribeiro, S. Pádua, J. C. Machado da Silva, and G. A. Barbosa, "Controlling the degree of visibility of Young's fringes with photon coincidence measurements," Phys. Rev. A **49**, 4176 (1994).
6. A. Gatti, E. Brambilla, and L. A. Lugiato, "Entangled imaging and wave-particle duality: from the microscopic to the macroscopic realm," Phys. Rev. Lett. **90**, 133603 (2003).
7. M. Ron, K. S. Deacon, and Y. H. Shih, "Ghost-imaging experiment by measuring reflected photons," Phys. Rev. A **77**, 041801 (2008).
8. J. Cheng and S.-H. Han, "Incoherent coincidence imaging and its applicability in X-ray diffraction," Phys. Rev. Lett. **92**, 093903 (2004).
9. A. F. Abouraddy, B. E. A. Saleh, A. V. Sergienko, and M. C. Teich, "Role of entanglement in two-photon imaging," Phys. Rev. Lett. **87**, 123602 (2001).
10. E. Baleine, A. Dogariu, and G. S. Agarwal, "Correlated imaging with shaped spatially partially coherent light," Opt. Lett. **31**, 2124 (2006).
11. X.-H. Chen, Q. Liu, K.-H. Luo, and L.-A. Wu, "Lensless ghost imaging with true thermal light," Opt. Lett. **34**, 695 (2009).
12. M. O. Scully and M. S. Zubairy, *Quantum Optics* (Cambridge University, 1999).
13. R. Hanbury Brown and R. Q. Twiss, "LXXIV. A new type of interferometer for use in radio astronomy," Lond. Edinb. Dublin Philos. Mag. J. Sci. **45**, 663 (1954).
14. R. Hanbury Brown and R. Q. Twiss, "Correlation between photons in two coherent beams of light," Nature **177**, 27 (1956).
15. R. Hanbury Brown and R. Q. Twiss, "A test of a new type of stellar interferometer on sirius," Nature **178**, 1046 (1956).
16. J. Cheng, "Ghost imaging through turbulent atmosphere," Opt. Express **17**, 7916 (2009).
17. F. Ferri, D. Magatti, L. A. Lugiato, and A. Gatti, "Differential ghost imaging," Phys. Rev. Lett. **104**, 253603 (2010).
18. X.-H. Chen, F.-H. Kong, Q. Fu, S.-Y. Meng, and L.-A. Wu, "Sub-Rayleigh resolution ghost imaging by spatial low-pass filtering," Opt. Lett. **42**, 5290 (2017).
19. P. A. Moreau, E. Toninelli, P. A. Morris, R. S. Aspden, T. Gregory, G. Spalding, R. W. Boyd, and M. J. Padgett, "Resolution limits of quantum ghost imaging," Opt. Express **26**, 7528 (2018).
20. S.-Y. Meng, Y.-H. Sha, Q. Fu, Q.-Q. Bao, W.-W. Shi, G.-D. Li, X.-H. Chen, and L.-A. Wu, "Super-resolution imaging by anticorrelation of optical intensities," Opt. Lett. **43**, 4759 (2018).
21. S. W. Hell and J. Wichmann, "Breaking the diffraction resolution limit by stimulated emission: stimulated-emission-depletion fluorescence microscopy," Opt. Lett. **19**, 780 (1994).
22. W. Larson and B. E. A. Saleh, "Resurgence of Rayleigh's curse in the presence of partial coherence," Optica **5**, 1382 (2018).
23. J. Du, W.-L. Gong, and S.-S. Han, "The influence of sparsity property of images on ghost imaging with thermal light," Opt. Lett. **37**, 1067 (2012).
24. W.-L. Gong and S.-S. Han, "Experimental investigation of the quality of lensless super-resolution ghost imaging via sparsity constraints," Phys. Lett. A **376**, 1519 (2012).
25. Y. Shechtman, S. Gazit, A. Szameit, Y. C. Eldar, and M. Segev, "Super-resolution and reconstruction of sparse images carried by incoherent light," Opt. Lett. **35**, 1148 (2010).
26. J. Chen, W.-L. Gong, and S.-S. Han, "Sub-Rayleigh ghost imaging via sparsity constraints based on a digital micro-mirror device," Phys. Lett. A **377**, 1844 (2013).
27. X. Bai, Y.-Q. Li, and S.-M. Zhao, "Differential compressive correlated imaging," Acta. Phys. Sin. **62**, 044209 (2013).
28. L.-Z. Li, X.-R. Yao, X.-F. Liu, W.-K. Yu, and G.-J. Zhai, "Super-resolution ghost imaging via compressed sensing," Acta. Phys. Sin. **63**, 224201 (2014).
29. P.-L. Zhang, W.-L. Gong, X. Shen, D.-J. Huang, and S.-S. Han, "Improving resolution by the second-order correlation of light fields," Opt. Lett. **34**, 1222 (2009).
30. J. Sprigg, T. Peng, and Y. H. Shih, "Super-resolution imaging using the spatial-frequency filtered intensity fluctuation correlation," Sci. Rep. **6**, 38077 (2016).
31. K. Kuplicki and K. W. C. Chan, "High-order ghost imaging using non-Rayleigh speckle sources," Opt. Express **24**, 26766 (2016).
32. Y.-L. Wang, Y.-N. Zhou, S.-X. Wang, F.-R. Wang, R.-F. Liu, H. Gao, P. Zhang, and F.-L. Li, "Enhancement of spatial resolution of ghost imaging via localizing and thresholding," Chin. Phys. B **28**, 044202 (2019).
33. Z.-S. Tong, Z.-T. Liu, C.-Y. Hu, J. Wang, and S.-S. Han, "Preconditioned deconvolution method for high-resolution ghost imaging," Photonics Res. **9**, 1069 (2021).
34. W-X. Shi, C.-Y. Hu, S.-G. Yang, M.-H. Chen, and H.-W. Chen, "Optical random speckle encoding based on hybrid wavelength and phase modulation," Opt. Lett. **46**, 3745 (2021).
35. F. Wang, C.-L. Wang, M.-L. Chen, W.-L. Gong, Y. Zhang, S.-S. Han, and G. Situ, "Far-field super-resolution ghost imaging with a deep neural network constraint," Light Sci. Appl. **11**, 1 (2022).
36. H.-L. Ye, Y. Kang, J. Wang, L.-H. Zhang, H.-J. Sun, and D.-W. Zhang, "High resolution reconstruction method of ghost imaging via SURF-NSML," J. Korean Phys. Soc. **80**, 964 (2022).
37. X. Zeng, Y.-F. Bai, X.-H. Shi, Y. Gao, and X.-Q. Fu, "The influence of the positive and negative defocusing on lensless ghost imaging," Opt. Commun. **382**, 415 (2017).
38. F. Ferri, D. Magatti, A. Gatti, M. Bache, E. Brambilla, and L. A. Lugiato, "High-resolution ghost image and ghost diffraction experiments with thermal light," Phys. Rev. Lett. **94**, 183602 (2005).
39. M. Paúr, B. Stoklasa, Z. Hradil, L. L. Sánchez-Soto, and J. Rehacek, "Achieving the ultimate optical resolution," Optica **3**, 1144 (2016).